Collective excitations and their lineshapes for a modulation-doped GaAs/AlAs superlattice

1994 J. Phys.: Condens. Matter 6 1553

(http://iopscience.iop.org/0953-8984/6/8/013)

J. Phys.: Condens. Matter 6 (1994) 1553–1562. Printed in the UK

Collective excitations and their lineshapes for a modulation-doped GaAs/AlAs superlattice

A C Sharma† and A K Sood‡§

† School of Studies in Physics, Jiwaji University, Gwalior-4740011, India
‡ Department of Physics, Indian Institute of Science, Bangalore-560012, India
§ Jawahar Lal Nehru Centre for Advanced Scientific Research, Indian Institute of Science, Campus, Bangalore-560012, India

Received 2 August 1993

Abstract. The density–density correlation function has been calculated for a modulation-doped GaAs/AlAs superlattice. The superlattice is modelled to be an infinite periodic sequence of layers which consists of two dissimilar layers, one of GaAs and the other of AlAs, per unit cell. The conduction electrons are assumed to be confined to GaAs layers. Our calculation shows that, although the electron gas is confined in the GaAs layers, the plasma oscillations can interact with the lattice vibrations of both GaAs and AlAs. The interaction between AlAs lattice vibrations and the plasmons significantly contributes to the light-scattering spectrum. It is therefore argued that the experimentally measured frequencies of the coupled plasmon–phonon modes and their lineshapes for a modulation-doped GaAs/AlAs superlattice cannot correctly be described by the previous theoretical calculations which have been performed for a layered electron gas embedded in a homogeneous dielectric background. For the special case of a homogeneous dielectric background, our results, however, agree with the previously reported calculations.

1. Introduction

The collective excitations, electronic as well as ionic, and the light scattering for collective excitations in semiconductor superlattices have been subjects of immense interest, ever since the discovery of this class of novel materials [1–17]. Extensive investigations, both experimental as well as theoretical, have been performed mainly for superlattices of type I, such as GaAs/$Al_xGa_{1-x}As$. Further, modulation-doped as well as undoped superlattices have been prepared to study the plasmons, the phonons, the plasmon–phonon coupled modes and the intensity of light scattered by these collective oscillations. Although numerous theoretical studies on plasmons and coupled plasmon–phonon modes in modulation-doped superlattices of type I exist, these studies have been performed by modelling the type I superlattices as an infinite one-dimensional (1D) array of either a purely two-dimensional (2D) electron gas or the electron gas layers embedded in a homogeneous polar dielectric host medium of dielectric constant $\varepsilon(\omega)$ [2–11]. However, the actual host medium which supports a layered electron gas (LEG) in a compositional superlattice is not homogeneous. It consists of alternate layers of two dissimilar polar semiconductors such as AlAs and GaAs in the case of the GaAs/AlAs superlattice. The host medium, therefore, supports two kinds of lattice vibration. One consists of bulk/interface longitudinal and transverse modes of the GaAs lattice, while the other belongs to bulk/interface longitudinal and transverse modes of AlAs. The light-scattering experiments performed on the undoped GaAs/AlAs superlattice

0953-8984/94/081553+10$19.50

clearly exhibit these two categories of lattice vibrational modes [12]. The plasma oscillations of the LEG can therefore interact with vibrational modes of both the GaAs and the AlAs layers. As the electron gas is mainly confined to the GaAs layers, plasma oscillations predominantly interact with lattice vibrations of GaAs. However, for certain values of the electron density, the width of a GaAs layer and the frequency and wavevector of light, the lattice vibrational modes of AlAs can also interact with the plasma oscillations to produce a significant change in the spectrum of the scattered-light intensity.

In this paper we report a theoretical calculation of the density–density correlation function (DDCF) for a modulation-doped GaAs/AlAs superlattice which is modelled to be a 1D periodic sequence of layers. Each period consists of two layers: one of GaAs and the other of AlAs. The conducting electrons are assumed to be confined in GaAs layers and to behave like free electrons with effective mass m^*. We further assume that the electron density is reasonably high in order to give rise to both intrasubband and intersubband plasmons. The unit cell of the system is constructed by taking two adjoining layers. Our calculation demonstrates that the intensity of scattered light for a LEG embedded in a heterogeneous dielectric background (HTDB), which comprises lattice vibrations of both GaAs and AlAs, consists of coupled intrasubband-plasmon–interface-phonon modes and the coupled intersubband-plasmon–interface-phonon modes. The frequencies and the lineshapes of these coupled plasmon–interface-phonon modes differ in a very obvious manner from the frequencies and the lineshapes of coupled plasmon–phonon modes which have been obtained previously from the calculated DDCF for a LEG embedded in a homogeneous dielectric background (HMDB) [3, 10]. Our calculation further shows that the plasma oscillations, which predominantly interact with lattice vibrations of GaAs for small electron densities and larger thicknesses of the GaAs layer, can also exhibit a strong interaction with the lattice vibrations of AlAs layers for a reasonably high electron density and small thickness of the GaAs layer. Thus, the interaction of plasma oscillations with the lattice vibrations of AlAs significantly contributes to the light-scattering spectrum of a modulation-doped GaAs/AlAs superlattice. Therefore, the existing calculations of the scattered-light intensity, which have been performed previously for a LEG in a HMDB, cannot correctly describe the experimental results on the light scattering in a modulation-doped compositional semiconductor superlattice such as a GaAs/AlAs superlattice. The remaining part of our paper is organized as follows. We present the calculation of the DDCF in section 2. In section 2, we discuss our results. Our work is then summarized in section 4.

2. Density–density correlation function and the lineshapes

The lineshapes for scattered light are determined from the imaginary part of the dynamical polarizability $\chi(q, \omega, z, z')$ which can be obtained by solving the integral equation [10]

$$\chi(q, \omega, z, z') = P(q, \omega, z, z') + \int\int dz_1\, dz_2\, P(q, \omega, z, z_1) V(q, z_1, z_2) \chi(q, \omega, z_2, z'). \quad (1)$$

Here, $P(q, \omega, z, z')$ is the polarizability in the absence of the Coulomb electron–electron interaction V which can be given as

$$V(q, z, z') = (2\pi e^2/q) \exp(-q|z - z'|). \quad (2)$$

We solve equation (1) for our model superlattice structure which consists of alternate layers of GaAs and AlAs along the z axis. We take d_1 as the thickness of the GaAs layer

and d_2 as the thickness of the AlAs layer. The length of the unit cell along the z axis, which is the sum of d_1 and d_2 is taken to be d. The ordinate of the lth layer can be defined as

$$z = ld + R_i + t \tag{3}$$

with

$$-\tfrac{1}{2}d_i \leqslant t \leqslant \tfrac{1}{2}d.$$

Here R_i is the distance of the ith layer of the lth unit cell measured from its bottom. As there are two layers in a unit cell, i can take two values. Further, the confinement of electrons in a GaAs layer generates the subband structure for electrons. Therefore, both intrasubband as well as intersubband transitions between different subbands are possible. One can use the diagonal approximation to decouple the different subband transitions [18]. For the n to m subband transition, we can transform equation (1) into [10]

$$\chi_{ij}^{nm}(q,\omega,l,l',t,t') = P_{ij}^{nm}(q,\omega,t,t')\delta_{ll'}\delta_{ij} + \sum_{l_1}\sum_{j'}\sum_{r}\iint \mathrm{d}t_1\,\mathrm{d}t_2 V_{ij'}(q,l,l_1,t,t_1)P_{jj}^{nr}(q,\omega,t_1,t_2) \times \chi_{j'j}^{rm}(q,\omega,l_1,l',t_2,t') \tag{4}$$

with

$$V_{ij}(q,l,l',t,t') = (2\pi e^2/q)\exp[-q|(l-l')d + R_{ij} + (t-t')|] \tag{5}$$

where $R_{ij} = R_i - R_j$. P_{jj}^{nm} is the total (electronic and ionic) polarizability of the jth layer.

Equation (4) is a matrix equation and χ_{ij}^{nm} is a 2×2 matrix in i and j. Further, each element of this 2×2 matrix forms a matrix in subband indices n and m. The size of the matrix in n and m is determined from the number of subbands which are to be considered in the calculation. For simplicity, we consider only two subbands (the ground and the first excited subband) and confine ourself to intrasubband transitions within the ground subband, and intersubband transitions between the ground subband and the first excited subband. We thus consider $0 \rightarrow 0$, $0 \rightarrow 1$ and $1 \rightarrow 0$ transitions. Each element of the matrix in i and j decomposes into two terms, one of which corresponds to intrasubband transitions, while the other corresponds to the intersubband transitions. Equation (4) can be simplified with the use of discrete Fourier transforms to obtain the lineshapes for different coupled plasmon–phonon modes. The lineshapes can be given by [11]

$$L(q,k_z,\omega) = \mathrm{Im}[\chi_{11}^{00}(q,\omega,k_z)+\chi_{12}^{00}(q,\omega,k_z)+\chi_{21}^{00}(q,\omega,k_z)+\chi_{22}^{00}(q,\omega,k_z)+\chi_{11}^{01}(q,\omega,k_z) + \chi_{12}^{01}(q,\omega,k_z) + \chi_{21}^{01}(q,\omega,k_z) + \chi_{22}^{01}(q,\omega,k_z)]. \tag{6}$$

Each term on the right-hand side of equation (6) can be written in terms of the 2D electronic polarizability (P_{1e}^{00}) for intrasubband transitions, the 2D electronic polarizability (P_{1e}^{01}) for

intersubband transitions, the ionic polarizability (P_{1i}) of GaAs and the ionic polarizability (P_{2i}) of AlAs as follows:

$$\chi_{11}^{00}(k_z) = A^{00}(k_z)[1 + V_{22}^{00}(k_z)P_{2i}](P_{1e}^{00} + P_{1i})/|\varepsilon^{00}(k_z)| \tag{7a}$$

$$\chi_{11}^{01}(k_z) = [1 + V_{22}^{00}(k_z)P_{2i}][A^{01}(k_z)P_{1e}^{01} + A^{00}(k_z)P_{1i}]/|\varepsilon^{01}(k_z)| \tag{7b}$$

$$\chi_{12}^{00}(k_z) = P_{2i}A^{00}(k_z)V_{12}^{00}(k_z)(P_{1e}^{00} + P_{1i})/|\varepsilon^{00}(k_z)| \tag{7c}$$

$$\chi_{12}^{01}(k_z) = P_{2i}[A^{01}(k_z)V_{12}^{01}(k_z)P_{1e}^{01} + A^{00}(k_z)V_{12}^{00}(k_z)P_{1i}]/|\varepsilon^{01}(k_z)| \tag{7d}$$

$$\chi_{21}^{00}(k_z) = P_{2i}A^{00}(k_z)V_{21}^{00}(k_z)(P_{1e}^{00} + P_{1i})/|\varepsilon^{00}(k_z)| \tag{7e}$$

$$\chi_{21}^{01}(k_z) = P_{2i}[A^{01}(k_z)V_{21}^{01}(k_z)P_{1e}^{01} + A^{00}(k_z)V_{21}^{00}(k_z)P_{1i}]/|\varepsilon^{01}(k_z)| \tag{7f}$$

$$\chi_{22}^{00}(k_z) = P_{2i}A^{00}(k_z)[1 + V_{11}^{00}(k_z)(P_{1e}^{00} + P_{1i})]/|\varepsilon^{00}(k_z)| \tag{7g}$$

$$\chi_{22}^{01}(k_z) = P_{2i}\{A^{00}(k_z)[1 + V_{11}^{00}(k_z)P_{1i}] + A^{01}(k_z)[1 + V_{11}^{01}(k_z)P_{1e}^{01}]/|\varepsilon^{01}(k_z)| \tag{7h}$$

with

$$A^{nm} = |\langle n|\exp(-ik_z t)|m\rangle|^2 \tag{8}$$

and

$$V_{ij}^{nm}(q, k_z) = (2\pi e^2/q)\{[H_{ij}^{nm}(q) - F_{ij}^{nm}(q)]\delta_{ij} + F_{ij}^{nm}(q)W_{ij}(q)\} \tag{9}$$

where

$$W_{ij}(q, k_z) = [\exp(-q|R_{ij}|)\exp(ik_z d)]/[\exp(ik_z d) - \exp(-qd)] + [\exp(q|R_{ij}|)\exp(-qd)]/[\exp(-ik_z d) - \exp(-qd)].$$

$W_{ij}(q, k_z)$ has the property $W_{ij}(q, k_z) \equiv W_{ji}(q, -k_z) \equiv W_{ji}^*(q, k_z)$. The matrix elements $H_{ij}^{nm}(q)$ and $F_{ij}^{nm}(q)$ are defined and their values are obtained in the appendix. In writing equation (7) the explicit q and ω dependences are suppressed for brevity. $|\varepsilon^{00}(q, \omega, k_z)|$ and $|\varepsilon^{01}(q, \omega, k_z)|$ are defined as

$$|\varepsilon^{00}(q, \omega, k_z)| = 1 + \alpha^0(q, k_z)[P_{1e}^{00}(q, \omega) + P_{1i}(q, \omega)] + \beta(q, k_z)P_{2i}(q, \omega) + [\alpha^0(q, k_z)\beta(q, k_z) - C_0(q, k_z)][P_{1e}^{00}(q, \omega) + P_{1i}(q, \omega)]P_{2i}(q, \omega) \tag{10}$$

$$|\varepsilon^{01}(q, \omega, k_z)| = 1 + \alpha^1(q, k_z)P_{1e}^{01}(q, \omega) + \alpha^0(q, k_z)P_{1i}(q, \omega) + \beta(q, k_z)P_{2i}(q, \omega) + [\alpha^1(q, k_z)\beta(q, k_z) - C_1(q, k_z)]P_{1e}^{01}(q, \omega)P_{2i}(q, \omega) + [\alpha^0(q, k_z)\beta(q, k_z) - C_0(q, k_z)]P_{1i}(q, \omega)P_{2i}(q, \omega) \tag{11}$$

where $\alpha^0(q, k_z)$, $\alpha^1(q, k_z)$, $\beta(q, k_z)$, $C_0(q, k_z)$ and $C_1(q, k_z)$ are defined as follows:

$$\alpha^0(q, k_z) = -(2\pi e^2/q)\{H_{11}^{00}(q) - F_{11}^{00}(q)[1 - S(q, k_z)]\} \tag{12a}$$

$$\alpha^1(q, k_z) = -(2\pi e^2/q)\{H_{11}^{01}(q) - F_{11}^{01}(q)[1 - S(q, k_z)]\} \tag{12b}$$

$$\beta(q, k_z) = -(2\pi e^2/q)\{H_{22}^{00}(q) - F_{22}^{00}(q)[1 - S(q, k_z)]\} \tag{12c}$$

$$C_0(q, k_2) = (2\pi e^2/q)^2 F_{12}^{00}(q)F_{21}^{00}(q)[R(q, k_z) + S^2(q, k_z)] \tag{12d}$$

$$C_1(q, k_z) = (2\pi e^2/q)F_{12}^{01}(q)F_{21}^{01}(q)[R(q, k_z) + S^2(q, k_z)] \tag{12e}$$

with

$$R(q, k_z) = -[\cosh(qd) - 1]/[\cosh(qd) - \cos(k_z d)] \tag{13a}$$

$$S(q, k_z) = \sinh(qd)/[\cosh(qd) - \cos(k_z d)]. \tag{13b}$$

As the main aim of this paper is to demonstrate the importance of proper inclusion of the effect of heterointerfaces in the dielectric background of the LEG, we here ignored the interaction between the intrasubband plasmons and the intersubband plasmons in order to avoid further complexity of our calculation. We believe that the inclusion of these effects will not significantly alter our main results. Further, as we are interested in the collective excitations which can be observed in the light-scattering experiments, we use the following long-wavelength limit of the random-phase approximation value of P_{1e}^{00}, P_{1e}^{01}, P_{1i} and P_{2i}:

$$P_{1e}^{00}(q, \omega) = -n_s q^2/\varepsilon_{100} m^* [\tfrac{1}{2}(q^2 v_F^2) - \omega(\omega + i\gamma_e)] \tag{14a}$$

$$P_{1i}^{01}(q, \omega) = -2n_s E_{10}/\varepsilon_{100} [E_{10}^2 - \omega(\omega + i\gamma_e)] \tag{14b}$$

$$P_{1i}(q, \omega) = -\{q^2(\omega_{L1}^2 - \omega_{T1}^2)/[\omega_{T1}^2 - \omega(\omega + i\gamma_{ph})]\}(d_1/4\pi e^2) \tag{14c}$$

$$P_{2i}(q, \omega) = -\{q^2(\omega_{L2}^2 - \omega_{T2}^2)/[\omega_{T2}^2 - \omega(\omega + i\gamma_{ph})]\}(d_2/4\pi e^2) \tag{14d}$$

n_s is the 2D carrier density. γ_e and γ_{ph} are the phenomenological broadenings for plasmons and phonons, respectively. ε_{100}, ω_{L1} and ω_{T1} are the optical dielectric constant, the longitudinal optical phonon frequency and the transverse phonon frequency, respectively, for GaAs. ε_{200}, ω_{L2} and ω_{T2} are the optical dielectric constant, the longitudinal optical phonon frequency and the transverse phonon frequency, respectively, for AlAs. E_{10} is the energy band gap between the ground subband and the first subband.

3. Results and discussion

The lineshapes for different coupled plasmon–phonon modes, which appear in the scattered-light spectrum, can be given by equation (6) for a modulation-doped GaAs/AlAs superlattice. The peak positions of these lineshapes represent the frequencies of different coupled plasmon–interface-phonon modes originating from the interaction between intrasubband plasmons, intersubband plasmons and lattice vibrations of GaAs and AlAs layers. The frequencies of coupled intrasubband plasmon–interface-phonon modes are given by the zeros in equation (10), while those of the intersubband plasmon–interface–phonon coupled modes are yielded by the zeros in equation (11). As is obvious from equation (6), our calculated $L(q, \omega, k_z)$ consists of four components of polarizability, i.e. χ_{11}, χ_{12}, χ_{21} and χ_{22}, while $L(q, \omega, k_z)$ for a LEG embedded in a HMDB consists of one polarizability component [9, 10]. As a special case, our calculation reduces to previous performed theoretical calculations of coupled plasmon–phonon modes and their lineshapes for a LEG in a HMDB [9, 10]. The third and fourth terms on the right-hand side of equation (10) and the third, fourth and fifth terms on the right-hand side of equation (11) are the contributions from the lattice vibrations of AlAs. For all values of the intrinsic parameters of a superlattice, our $L(q, \omega, k_z)$ computed using equation (6) differ significantly from the previously computed $L(q, \omega, k_z)$ of a LEG embedded in a HMDB [9, 10].

In order to demonstrate the importance of proper consideration of the lattice vibrations of AlAs in the theoretical study of coupled plasmon–phonon modes for a modulation-doped GaAs/AlAs superlattice, we computed the peak position and the peak height of different coupled plasmon–phonon modes, for several values of n_s. The peak positions of the intrasubband plasmon–interface-phonon coupled modes L_1, L_2 and L_3 and the peak positions of the intersubband plasmon–interface-phonon coupled modes I_1, I_2 and I_3 are plotted as functions of n_s in figure 1. For the computation, we used $E_{10} = 21.7$ eV, $\varepsilon_{100} = 10.9$, $\varepsilon_{200} = 8.2$, $\omega_{L1} = 295$ cm^{-1}, $\omega_{T1} = 273$ cm^{-1}, $\omega_{L2} = 405$ cm^{-1}, $\omega_{T2} = 364$ cm^{-1}, $d_1 = 200$ Å, $d_2 = 204$ Å, $qd = 1$, $2k_zd = 5.656$, $m^* = 0.068m_e$, $\gamma_e = 1.26$ cm^{-1} and $\gamma_{ph} = 0.81$ cm^{-1}. In our numerical computation, we used $2k_zd$ in place of k_zd, for the reasons mentioned in [9]. From figure 1, we note the following.

(i) L_1, L_2, L_3, I_1, I_2 and I_3 vary with n_s, demonstrating that the plasma oscillations interact with lattice vibrations of both GaAs and AlAs, although the electron gas is confined to GaAs layers.

(ii) Our computed $L(q, \omega, k_z)$ consists of coupled plasmon–interface-phonon modes; it does not exhibit coupled plasmon–bulk-phonon modes.

(iii) I_2 and I_3 show stronger n-dependences than do L_2 and L_3, respectively, indicating that the interaction between intersubband plasmons and interface phonons is stronger than that between intrasubband plasmons and interface phonons.

(iv) L_1, L_2, L_3, I_1 and I_2 increase on increasing n_s, while I_3 decreases on increasing n_s, as can be seen from the figure.

(v) The lattice vibrations of GaAs interact more strongly, in comparison with the lattice vibrations AlAs, with both types of plasmon.

We plot the frequencies of the coupled phonon–phonon modes in figure 2(a), of the coupled intrasubband plasmon–phonon modes in figure 2(b) and of the coupled intersubband plasmon–phonon modes in figure 2(c), as functions of qd, for all possible values of $\cos(k_zd)$. We used $n_s = 4.2 \times 10^{11}$ cm^{-2} to compute both the coupled intrasubband and the coupled intersubband plasmon–phonon modes. The bands of coupled phonon–phonon modes which are shown in figure 2(a) consist of low-energy interface phonon modes, observed in the light-scattering experiments performed by Sood *et al* [13]. However, the semiclassical calculations of phonon modes, which employed the matching of electrostatic potential at the periodic heterointerfaces of a superlattice, gives rise to four interface phonon bands [6, 16]. For q tends to zero, the energies of two of the bands (the low-energy interface-phonon modes) approach the transverse bulk-phonon energies, while the energies of the other two bands (the high-energy interface-phonon modes) approach the energies of longitudinal bulk phonons. From our calculation, we obtain only low-energy interface phonons. This might be due to the several simplifying approximations used in our calculation. A more elaborate calculation may give rise to bands of all four interface-phonon modes. However, our calculation of the DDCF is quite general in nature and it can easily be extended to explore all types of the interface- and bulk-phonon modes in a superlattice structure. The interaction of low-energy interface phonons with the intrasubband and intersubband plasmons can be visualized from figures 2(b) and 2(c). It is obvious from the figures that the interface phonons show a stronger interaction with intersubband plasmons than with the intrasubband plasmons, for all values of qd and k_zd. We have noted the changes in the GaAs-like interface phonon frequency due to the interaction with intrasubband plasmons (ΔL_2) and with intersubband plasmons (ΔI_2) and the changes in the AlAs-like interface phonon frequency because of the interaction with intrasubband plasmons (ΔL_3) and with intersubband plasmons (ΔI_3) for several values of qd, k_zd and n_s. We find that, for given

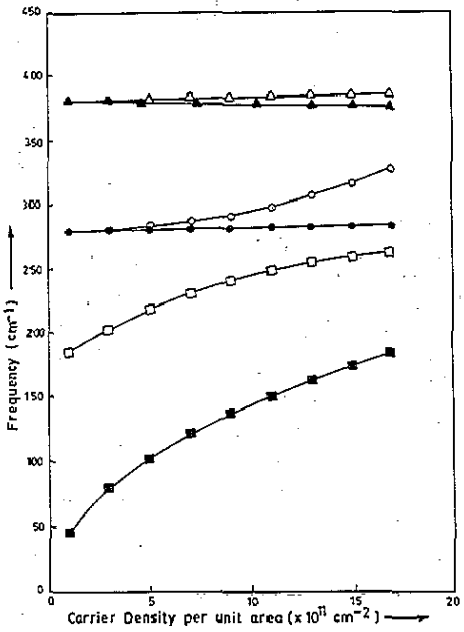

Figure 1. Plots of L_1 (■), I_1 (□), L_2 (●), I_2 (○), I_3 (▲) and L_3 (△) versus carrier density n_s.

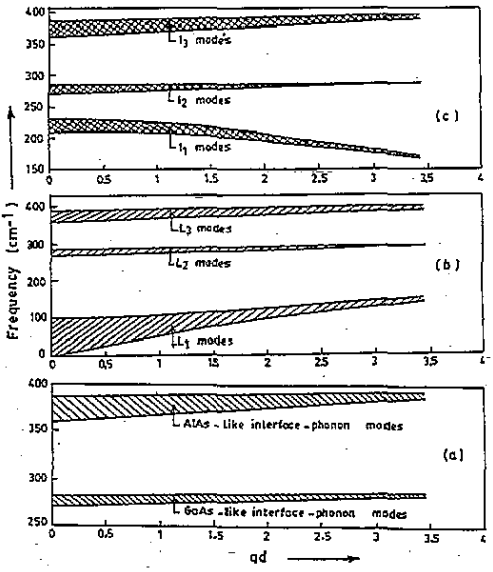

Figure 2. The energies of (*a*) GaAs-like and AlAs-like phonon modes, (*b*) coupled intrasubband-plasmon–interface-phonon modes L_1, L_2 and L_3 and (*c*) coupled intersubband-plasmon–interface-phonon modes I_1, I_2 and I_3 plotted as functions of qd for all possible values of $\cos(k_z d)$.

values of n_s and qd, ΔL_2, ΔI_2, ΔL_3 and ΔI_3 exhibit their maximum values at $k_z d = 0$. For $k_z d = \pi$, ΔL_2, ΔI_2, ΔL_3 and ΔI_3 are almost zero, for all values of qd and n_s. We further noted that, for $k_z d = 0$, ΔL_2 varies between 1 and 3 cm^{-1}, $\Delta I_2 \simeq 2$ cm^{-1}, ΔL_3 varies between 4 and 0 cm^{-1} and $\Delta I_3 \simeq -1$ cm^{-1}, on varying qd from 0.01 to 3.5 at $n_s = 4.2 \times 10^{12}$ cm^{-2}. Also, the bands of L_2 and L_3 overlap with the bands of I_2 and I_3 respectively, for a certain range of qd-values, at small n_s.

$L(q, \omega, k_z)$ from equation (6) for a LEG embedded in a HMDB is plotted as a function of ω in figure 3(*a*) for $n_s = 4.2 \times 10^{11}$ cm^{-2} and in figure 3(*b*) for $n_s = 1.26 \times 10^{12}$ cm^{-2}. The values of the rest of the parameters are those which have been used to obtain figure 1. Figures 3(*a*) and 3(*b*) clearly demonstrate the effect of proper consideration of the HTDB (the dielectric mismatch at the heterointerfaces) in the calculation of the light-scattering spectrum. From the figures, one can clearly distinguish between the intrasubband–intersubband plasmon lineshape for a LEG in a HMDB and the corresponding plasmon lineshape for a LEG in a HTDB. The difference is much more obvious for higher values of n_s, as can be seen from figure 3(*b*). We note that both intrasubband and intersubband plasmon frequencies for a LEG in a HTDB are higher than those for a LEG in a HMDB. Further, the change in the intersubband plasmon frequency is larger than that in the intrasubband plasmon frequency. This further illustrates that the intersubband plasmons interact more strongly with the lattice vibrations of dielectric background. Also, we note from figure 3 that the peak heights of various lineshapes for a LEG in a HMDB are higher than those for a LEG in a HTDB.

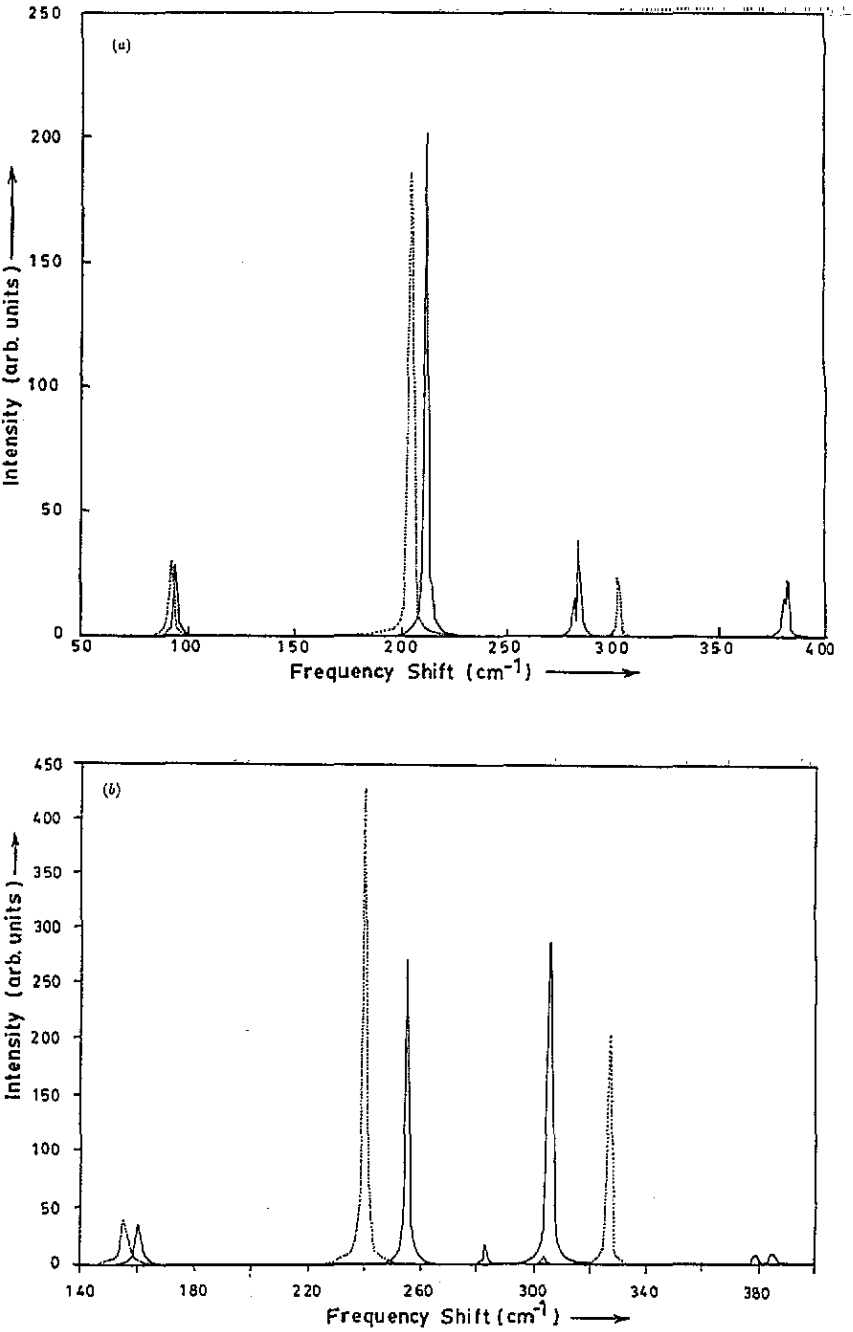

Figure 3. (*a*) The imaginary part of $L(q, k_z, \omega)$ for a LEG in a HMDB dielectric background (dotted) and for a LEG in a HTDB dielectric background (——) plotted as a function of ω for $n_s = 4.2 \times 10^{11}$ cm^{-2}. (*b*) The imaginary part of $L(q, k_z, \omega)$ for a LEG in a HMDB (·····) and for a LEG in a HTDB (——) plotted as a function of ω for $n_s = 1.26 \times 10^{12}$ cm^{-2}.

4. Conclusions

We calculated $L(q, \omega, k_z)$ for a modulation-doped GaAs/AlAs superlattice which is modelled to be a 1D infinite array of electron gas layers embedded in a HTDB which consists of alternate layers of two dissimilar polar dielectrics. We found that, for all values of n_s, the positions and heights of peaks of various lineshapes which belong to coupled plasmon–phonon modes of a LEG in a HTDB significantly differ from those of a LEG in a HMDB. The calculated light-scattering spectrum for a LEG in a HTDB consists of coupled plasmon–interface-phonon modes, while the calculated light-scattering spectrum for a LEG in a HMDB exhibits coupled plasmon–bulk-phonon modes. Also, the lineshape which corresponds to a intrasubband/intersubband plasmon mode of a LEG in a HTDB clearly differs from that of a LEG in a HMDB. Although the AlAs lattice vibrations interact with both intrasubband and intersubband plasmons, their interaction with intersubband plasmons is more prominent. The lineshapes belonging to L_2 and L_3 approximately coincided with those belonging to I_2 and I_3 respectively, for small values of n_s. In conclusion, we have shown that the calculated light-scattering spectrum of a LEG in a HTDB significantly differs from the calculated light-scattering spectrum of a LEG in a HMDB. It will be desirable to understand the existing data [20] as well as to carry out fresh experiments to look for the predicted effects.

Acknowledgments

This work was done during the visit of ACS to the Indian Institute of Science, Bangalore. He acknowledges with thanks the financial support from Madhya Pradesh Council of Science and Technology, Bhopal, for the visit and the Department of Physics, Indian Institute of Science, Bangalore, for hospitality. ACS thanks the University Grants Commission, New Delhi, and AKS thanks the Department of Science and Technology, for financial assistance.

Appendix

The $H_{ij}^{nm}(q)$ are defined by

$$H_{ij}^{nm}(q) = \int_{-d_i/2}^{d_i/2} \mathrm{d}t \int_{-d_i/2}^{d_i/2} \mathrm{d}t' \exp(-q|t-t'|)\psi_{mn}(t)\psi_{mn}(t'). \tag{A1}$$

$F_{ij}^{nm}(q)$ is given by equation (A1) on replacing $q|t-t'|$ by $q(t-t')$. $\psi_{nm}(t)$ is the product of the envelope functions of the nth and mth subbands. H_{ij}^{00}, H_{ij}^{01}, F_{ij}^{00}, F_{ij}^{01}, A^{00} and A^{01} are evaluated using the following infinite deep-potential-well wavefunctions [19]:

$$\psi_\lambda(Z) = (2/d_i)\sin^2[(\lambda+1)\pi(Z/d_i + \tfrac{1}{2})] \tag{A2}$$

where λ is the composite index. For the $0 \to 0$ transition, $\lambda = 0$ and for $0 \to 1$ or $1 \to 0$, $\lambda = 1$. On evaluating equation (A1), one obtains

$$H_{ii}^{\lambda}(q) = u_i[1/x_\lambda + (1+\delta_{\lambda 0})/y_\lambda] - 2u_i^2\{\pi^2[(\lambda+2)^2 - \lambda^2]/x_\lambda y_\lambda\}^2[1-(-1)^\lambda \exp(-u_i)]. \tag{A3}$$

Similarly, one obtains

$$F_{ij}^{\lambda}(q) = f_i^{\lambda}(q) f_j^{\lambda}(-q) \tag{A4}$$

$$f_i^{\lambda}(q) = u_i\pi^2\{[(\lambda+2)^2 - \lambda^2]/x_\lambda y_\lambda\}[1-(-1)^\lambda \exp(-u_i)] \tag{A5}$$

with $u_i = qd_i$, $x_\lambda = u_i^2 + \pi^2(\lambda+2)^2$ and $y_\lambda = u_i^2 + \pi^2\lambda^2$. A^{00} and A^{01} can be obtained from F_{11}^{00} and F_{11}^{01}, respectively, on replacing u_i by ik_zd_i.

References

[1] Olego D, Pinczuk A, Gossard A C and Weigmann W 1982 *Phys. Rev.* B **25** 7867–71
[2] Jain J K and Allen P B 1985 *Phys. Rev. Lett.* **54** 947–1004
Jain J K and Das Sarma S 1987 *Phys. Rev.* B **36** 5949–52
[3] Tselis A C and Quinn J J 1984 *Phys. Rev.* B **29** 3318–35
[4] Bloss W L 1991 *Phys. Rev.* B **44** 1105–12
[5] Das Sarma S and Madhukar A 1981 *Phys. Rev.* B **23** 805–15
[6] Camley R E and Mills D L 1984 *Phys. Rev.* B **29** 1695–706
[7] Zhu X, Xia X, Quinn J J and Hawrylak P 1988 *Phys. Rev.* B **38** 5617–23
[8] Sharma A C 1991 *Mod. Phys. Lett.* B **5** 455–63
[9] Hawrylak P, Wu J and Quinn J J 1985 *Phys. Rev.* B **32** 5169–76
[10] Katayama S and Ando T 1985 *J. Phys. Soc. Japan* **54** 1615–26
[11] Tozoar N and Zhang C 1986 *Phys. Rev.* B **34** 1050–6
[12] Sood A K 1989 *Defence Sci. J.* **39** 411–23; 1989 *Vibrational Spectra and Structure* vol 17, ed H D Bist, J R Durig and J F Sullivan (Amsterdam: Elsevier) pp 295–301, and references therein
[13] Sood A K, Menendez J, Cardona M and Ploog K 1985 *Phys. Rev. Lett.* **54** 2111–14; 2115–18
[14] Lambin Ph, Vigneron J P and Lucas A A 1985 *Phys. Rev.* B **32** 8203–15
[15] Pokatilov E P and Beril S I 1983 *Phys. Status Solidi* b **188** 567–73
[16] Bechstedt F and Ederlein R 1985 *Phys. Status Solidi* b **131** 53–66
[17] Lambin Ph, Vigneron J P, Lucas A A, Thiry P A, Liehr M, Pireaux J J, Caudano R and Kuech T J 1986 *Phys. Rev. Lett.* **56** 1842–5
[18] Dahl D L and Sham L J 1977 *Phys. Rev.* B **16** 651–69
[19] Hawrylak P, Jie-Wei Wu and Quinn J J 1985 *Phys. Rev.* B **31** 7855–8
[20] Sood A K, Cardona M, Fischer A and Ploog K 1989 *Raman Spectroscopy* ed S B Banerjee and S S Jha (Singapore: World Scientific) pp 289–93